Sustainable Energy & Fuels

Polysulfides Mitigation through Tailored Separator for Critical Temperature Energy-Dense Lithium-Sulfur Batteries

Journal:	*Sustainable Energy & Fuels*
Manuscript ID	SE-ART-06-2022-000767.R1
Article Type:	Paper
Date Submitted by the Author:	08-Oct-2022
Complete List of Authors:	Parekh, Mihit; Purdue University, Davidson School of Chemical Engineering Rao, Harsha; Purdue University Jokhakar, Deep; Purdue University, Davidson School of Chemical Engineering Parikh, Vihang; Purdue University, Chemical Engineering Palanisamy, Manikandan; University of Tennessee Knoxville College of Engineering, School of Chemical Engineering; Pol, Vilas; Purdue University, Davidson School of Chemical Engineering

Polysulfides Mitigation through Tailored Separator for Critical Temperature Energy-Dense Lithium-Sulfur Batteries

Mihit H.Parekh,[a,*] Harsha Rao,[a] Deep Jokhakar,[a,b] Vihang P.Parikh,[a] Manikandan Palanisamy,[a] Vilas G. Pol[a,*]

[a]Davidson School of Chemical Engineering, Purdue University, West Lafayette, IN 47907

[b]Brightvolt Incorporation, 7970 S Energy Dr, Newberry, IN 47449

***Corresponding authors** – Vilas G. Pol, email address: vpol@purdue.edu;

Mihit H. Parekh, email address: parekhm@purdue.edu

Abstract

Sulfur is one of the promising next-generation cathodes owing to its light weight, abundance, cost, and above all extremely high theoretical capacity. However, the chemistry suffers from critical issues viz., poor sulfur conductivity, polysulfide shuttling, and lithium dendrite growth. Here, through the use of a tailored separator, comprising of graphene-polydopamine coat on a standard Celgard polypropylene separator, all the issues were tackled simultaneously. Functionalized separator acted as a barricade for polysulfide from shuttling by adsorbing them preferably due to their favorable interactions with functional groups of polydopamine on the surface and outperformed the pristine separator. At –25, 0, 25, 40, and 50 ℃, the cells yielded about 170, 350, 580, 360, and 550 mAh g^{-1} capacity, respectively. The system delivered 100 cycles at 50 ℃ followed by 300 cycles at 40 ℃. The capacity retention of 95% at 0.5C was reported after being exposed to high rates of 3C and 4C. A similar stable performance was observed with single-layered pouch cells. High-performance Li-S batteries proposed here can be valuable to a variety of applications like defense, transportation, and space explorations, where drastic conditions affect the battery functionalities, in the coming times ahead.

Keywords: Li-S batteries, low temperature, tailored separator, polydopamine

1. Introduction

Lithium-ion batteries (LIBs) are one of the technologies that have revolutionized human life beyond imagination.[1, 2] We have become heavily dependent on them for our day-to-day affairs. LIBs have been incorporated into portable consumer appliances, defense applications, and electric vehicles (EVs).[3] In LIBs, various high theoretical specific capacity anode materials like silicon (3596 mAh g^{-1}),[4] tin (993 mAh g^{-1}), antimony (660 mAh g^{-1}), carbon (372 mAh g^{-1}),[5] and their composites have been extensively developed in the past thirty years. Subsequently, promising cathode materials like $LiCoO_2$, $LiMn_xNi_yCo_zO_2$ (x+y+z = 1), $LiFePO_4$, $LiMn_2O_4$ have been used.[6] However, the practical specific capacities of these cathodes are < 250 mAh g^{-1},[7] and hence thicker cathodes are required to match with the anodes' capacities. Thicker cathode comes with several issues of capacity fade due to high overpotentials during cycling, high impedance for electrons, higher current densities on separators (causing more overpotentials), potential lithium plating, and impedes the mass transfer of Li^+ ions.[8, 9] Also, LIBs cannot cope with the ever-increasing demand for more power and energy-consuming applications like energy grids, electric vehicles (EVs), wearable electronics, etc.[10] This would require a significant increment in the energy density, capacity, and reduction in the cost of raw materials of the system. In this scenario, sulfur can be used as one of the alternative cathodes in the lithium-ion shuttling system for high-power applications.[3]

Sulfur is the lightest cathode, and has attractive properties viz., the high theoretical specific capacity of 1672 mAh g^{-1}, high energy density (2600 Wh kg^{-1}), abundant, and inexpensive (~$50 per metric ton).[11] Other advantages of transitioning from conventional insertion cathodes to sulfur apart from high capacity are eco-friendly nature and improved safety from the lower operational voltage (2.15 V vs Li/Li^+). Sulfur would have a crucial role to play for advanced next-generation batteries.[12] Sulfur chemistry is quite old, about 50 years back it was used as primary batteries, and since the last decade has garnered attention as an inexpensive alternative to rechargeable Li^+ ion technologies. There are a few critical issues to be dealt with before the goal can be realized viz., the electrically insulative nature of sulfur (5×10^{-30} S cm^{-1} at 25 °C), volume expansion effects, polysulfide shuttling effect, and dendritic growth of metallic lithium.[3, 12-14] Low conductivity of sulfur generates inadequate electrochemical contact of active material, increased internal battery resistance, and subsequently, large polarization. Octasulfur (cyclo-S_8) undergoes morphological

and structural transformations during the redox process to form insoluble, and poor ionic conductive short-chain polysulfides i.e., Li_2S & Li_2S_2, and soluble long-chain polysulfides i.e., Li_2S_X ($8 \leq X \leq 3$) in liquid electrolyte. The insoluble polysulfides on the sulfur surface prevent further reduction in discharging process and the soluble polysulfides shuttle across the separator. These unwanted characteristics lead to inefficient active material utilization, poor safety assurance, poor system energy efficiency, and drastically low cycle life.[15-18]

To tackle the conductivity issue of sulfur and polysulfide shuttling effect, the following approaches have been taken a) impregnation of sulfur in mesoporous materials like carbon;[19-21] b) using metal sulfides or oxides, which form bonds with polysulfides;[22-25] c) coating sulfur with conductive polymers;[26] d) using metallic organic frameworks or covalent organic frameworks;[27-29] e) inverse vulcanization using sulfur as the main chain;[30, 31] f) fabricate cathode comprising of SeS.[32, 33] However, some of these approaches, lead to lowering of the energy density of the system, involve complex fabrication steps or raw materials are expensive. To address the issue of lithium metal dendrites growth, exotic electrode coatings, electrolytic additives, and special shutdown separators are used.[34-36] Nevertheless, the specified approaches impede cell performance in line with high-cost procedures. Therefore, an alternative commercially viable approach is modifying the polypropylene (PP) separator, as it can easily resolve the coulombic efficiency issue of Li-metal batteries, and cycle performance at critical temperatures.[37, 38]

Herein, we report the proposed hypothesis that, the use of surface tailored separator for sulfur-carbon (SC) cathode for trapping polysulfide, curbing dendrites growth, and mitigating their propagation. In previous studies, it has been reported that polydopamine (PDA) coated separators have better ionic conductivity and wettability and positively affect electrochemical performance.[39, 40] Then the graphene coating on the PDA-coated separator supports accommodating volume expansion of SC electrode during cycling as well as enhancing local electrical conductivity. The tailored separator acted as a barrier in preventing the shuttling of polysulfide by adsorbing them preferentially due to the unique characteristic of the hydrophilic nature of the separator.

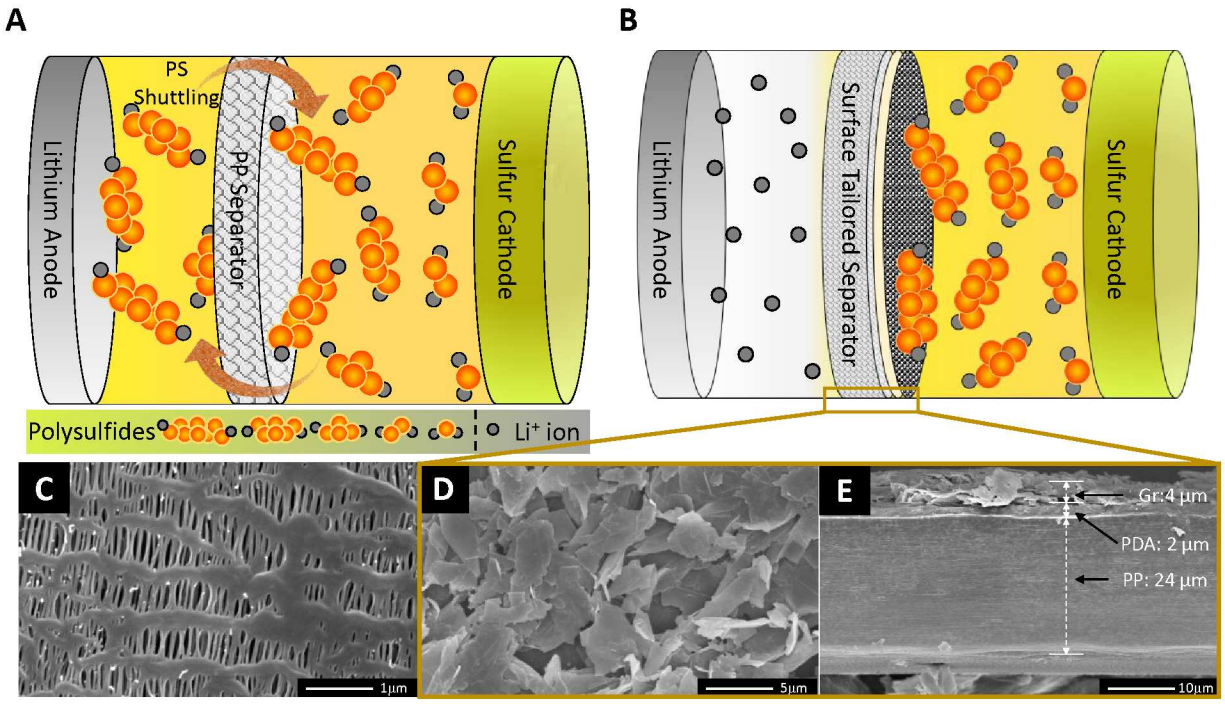

Figure 1: Schematic representation of LiS chemistry in batteries. A: Presence of polysulfide shuttling effect in presence of polypropylene separator; B: Suppression of polysulfide shuttling effect with the presence of tailored separator. High resolution scanning electron microscopy of separators, C: Top-view of polypropylene separator, D: Top-view of tailored separator containing graphene particles, and E: Cross-sectional view of the tailored separator illustrating graphene, and polydopamine layers on polypropylene separator.

2. Results & Discussion

Figure 1 shows a schematic of LiS batteries in presence of a conventional PP separator and tailored separator. In a conventional setup, shown in Fig. 1A, the polysulfides easily shuttle across the separator leading to a reduction in coulombic efficiency and side reactions on the anode surface. Also, the dendritic growth occurs on the surface of Li, which can eventually pierce through the separator causing short-circuit and leading to fire or explosion in extreme cases. However, the tailored separator, which has layers of polydopamine, and graphene behaves like a physical barrier to block the shuttling of polysulfides, as shown in Fig. 1B. Figure C-E depicts high-resolution SEM images of polypropylene separator, top view, and cross-sectional view of the surface tailored separator. Flaky-natured graphene coated on the PP separator can be observed in Fig. 1D. The polydopamine layer on PP is ~2 µm with the majority of PDA imbibed inside the PP separator, and the graphene-CMC binder coating on the PDA layer is about 4 µm. The thinner layers facilitate the easy exchange of Li^+ ions across the separator.

X-ray diffraction, Raman spectroscopy, BET adsorption, and DLS particle size distribution was performed on the carbon-sulfur composite material to study the phase purity, crystallinity, porosity and surface area, and particle size distribution, respectively. To understand the effect of temperature on the ionic conductivity of the electrolyte, it was analyzed on Autolab Microcell HC with TSC1600 cell. Figure 2A shows the XRD pattern of SC composite. In comparison with JCPDS # 83-2283, the crystal structure of the sulfur appears to be Fddd orthorhombic with major characteristic peaks appearing at 23.06°, 25.86°, and 27.72°.[41, 42] Raman spectra of the SC composite and elemental sulfur are shown in Fig. 2B. For elemental sulfur, characteristic bands are observed at 155, 220, and 474 cm^{-1}. For SC composite, there are characteristic bands seen at 1324 and 1592 cm^{-1}, which are occurring from the resonance of D-band and G-band stretching of carbon.[43] The features of sulfur are suppressed by the bands of carbon with a slight bulge being noticed in the lower range of wavenumber. The XRD pattern and Raman spectrum of graphene used for tailored separator are shown in Figure S1.

Figure 2C shows nitrogen adsorption isotherms for SC composite and it represents a mixed type I and II isotherms based on the relative pressure (P/P_0). At high P/P_0, the majority volume is adsorbed indicating macroporous or non-porous structure. In the low and intermediate P/P_0 range, the adsorption is due to the microporous structure of C-65 and the outer mesoporous surface, respectively. The Brunauer–Emmett–Teller (BET) surface area of the SC composite was found to be 11.35 $m^2\ g^{-1}$. From the pore size distribution, the composite exhibits micropores (<2 nm), mesopores (2–5 nm), and medium coarse mesopores (>10 nm) distribution (Fig. 2D). This suggests that there might be pore accumulation occurrence in the composite. The hand-milled SC composite was characterized by NanoBrook 90Plus PALS analyzer, where the sample was dispersed in ethanol and sonicated to break the aggregates. The d_{90} value of the SC composite is 131 nm as illustrated in Fig. 2E.

As Li-S chemistry requires a combination of specific solvent(s), lithium salt(s), and additives(s) to function in operating voltage range while having stability with pure lithium metal, we prepared an in-house electrolyte with 1M LiTFSI in 1:1 (v/v) DOL:DME with 1 wt% $LiNO_3$. To characterize this electrolyte, conductivity at various temperatures was measured to calculate Arrhenius parameters and compared with other electrolytes reported in the literature. Autolab Microcell HC has the ability of a typical potentiostat and combines a temperature-controlled chamber with a cell. Measurement of EIS at OCV with frequency in the range of 1 MHz to 1 Hz at various temperatures

was done. Conductivity calculations are based on the charge transfer resistance. The EIS at room temperature and Arrhenius plot are shown below in Fig. 2F. A linear fitting provides the slope, which is equal to the ratio of activation energy and gas constant. Based on our experiment, activation energy is 0.073 eV, and this is comparable to values available in the literature.[44] Hence, the control experiment is comparable to other studies.

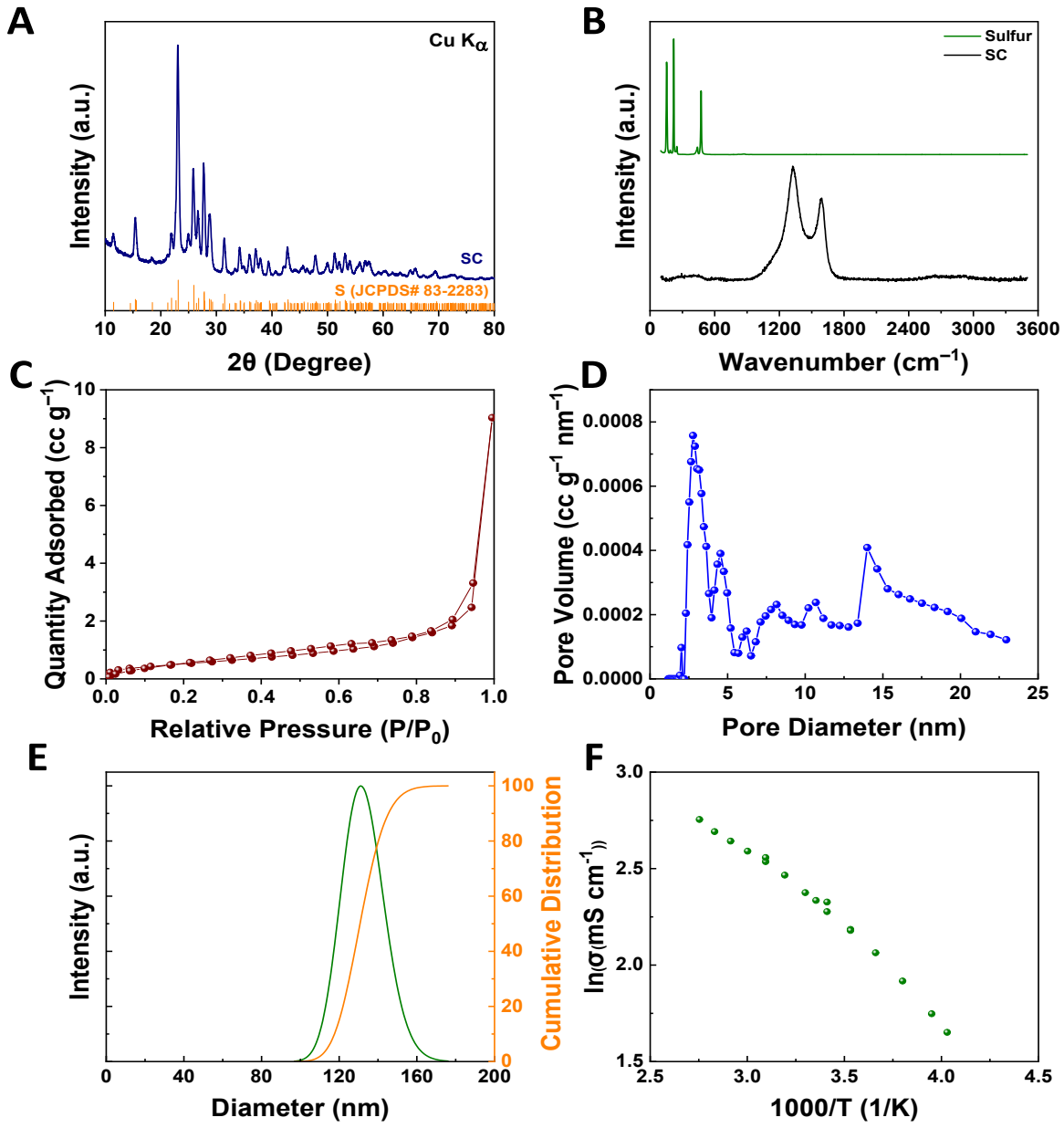

Figure 2: A: XRD patterns of SC, Sulfur; B: Raman Spectra of SC composite, and sulfur; C: Adsorption isotherm for SC composite; D: Pore size distribution of SC composite, E: PALS Particle size distribution for the SC composite; and F: Conductivity of the electrolyte at different temperatures.

Figure 3 shows the electrochemical performance of the SC cathode with a tailored separator and with a pristine separator at room temperature, 25 ℃. The cyclic voltammetry of SC cathode in the presence of a pristine and tailored separator are depicted in Fig. S2, and Fig. 3A, respectively. Though the anodic process of the Li extraction is simple and is analogous to other carbon-based cathodes, however, the cathodic process is divided into multiple redox steps for the Li insertion. Two reduction peaks are observed around 2.04V and 2.3V. In Fig. 3A, overlapping oxidation peaks are observed between 2.33 and 2.55 V. To analyze the interfacial behaviors of each sulfur electrode, electrochemical impedance spectroscopy (EIS) studies were carried out. The Ohmic resistance (R_s) of pristine (Fig. S3), and tailored separators (Fig. 3B) showed values of 5.1 Ω, and 2.5 Ω, respectively. The charge transfer resistance (R_{ct}) of each cell exhibited different values. The pristine separator cell showed a higher charge transfer resistance (22.3 Ω), compared with the tailored separator cell (12.8 Ω), indicating that the electrical conductivity of the cathode is enhanced by the presence of graphene-PDA coated separator.[45] Also, tailored separator cells showed a prominent Warburg diffusion element as compared to pristine separator cells.

Figure 3C demonstrates rate studies of SC cathode showing the specific capacities. Multi-rate galvanostatic cycling is exhibited at different rates between 0.1C and 4C. As can be seen in Fig. 3C, the capacity retention for 0.5C was ~ 93%. The tailored separator exhibited capacities of 925, 833, 644, 480, 326, 260, and 220 mAh g^{-1} at increasing C rates. Capacity retention for 0.5C rate was ~95%. Conversion-type cathode materials are less suited for fast charging applications and therefore, stellar performance is not observed above 2C.[46] A similar deterioration of capacity during fast charging is observed with a pristine separator (Figure S4). Figure 3D and Figure S5 show the charge-discharge voltage characteristics of SC composite with tailored separator, and pristine separator at 0.5C rate, respectively. Two discharge plateaus are observed at 2.38 V and 2.06 V, which are congruent to the cathodic peaks seen in CV. At 0.5C rate, the tailored separator exhibited a high charge-discharge capacity of 677/687 mAh g^{-1} compared to the cell with 663/713 mAh g^{-1} of the pristine separator, shown in Fig. 3E. This drastic difference in the performance of cells by change in separators may be due to the formation of polysulfides pre-cycling, as a dark yellowish colored ring is observed around the SC composite electrode. The presence of graphene and polydopamine in the tailored separator prevents the polysulfides from shuttling across the separator by the physical adsorption phenomenon. Dopamine contains amine and catechol groups, which generate a hydrophilic environment on the surface of the PP separator and improves its

wettability (Figure S6), uptake, and conductivity.[47] The hydrophilic surface allows for the facile coating of graphene with Na-CMC binder on the PDA-coated PP separator. This hydrophilic natured graphene-PDA layer can successfully adsorb the polar polysulfides (typically long-chain polysulfides).[48] The layer prevents the diffusion of polysulfides and also acts as a buffer to accommodate volume changes in the SC cathode. The coating of PDA on the PP separator blocks the channels on it, which in conventional separator provides the pathway for polysulfide dispersion. Figure S7 shows the top view of PDA coated PP separator. Furthermore, the effect of a tailored separator on the suppression of polysulfide diffusion is demonstrated in Figure S8.

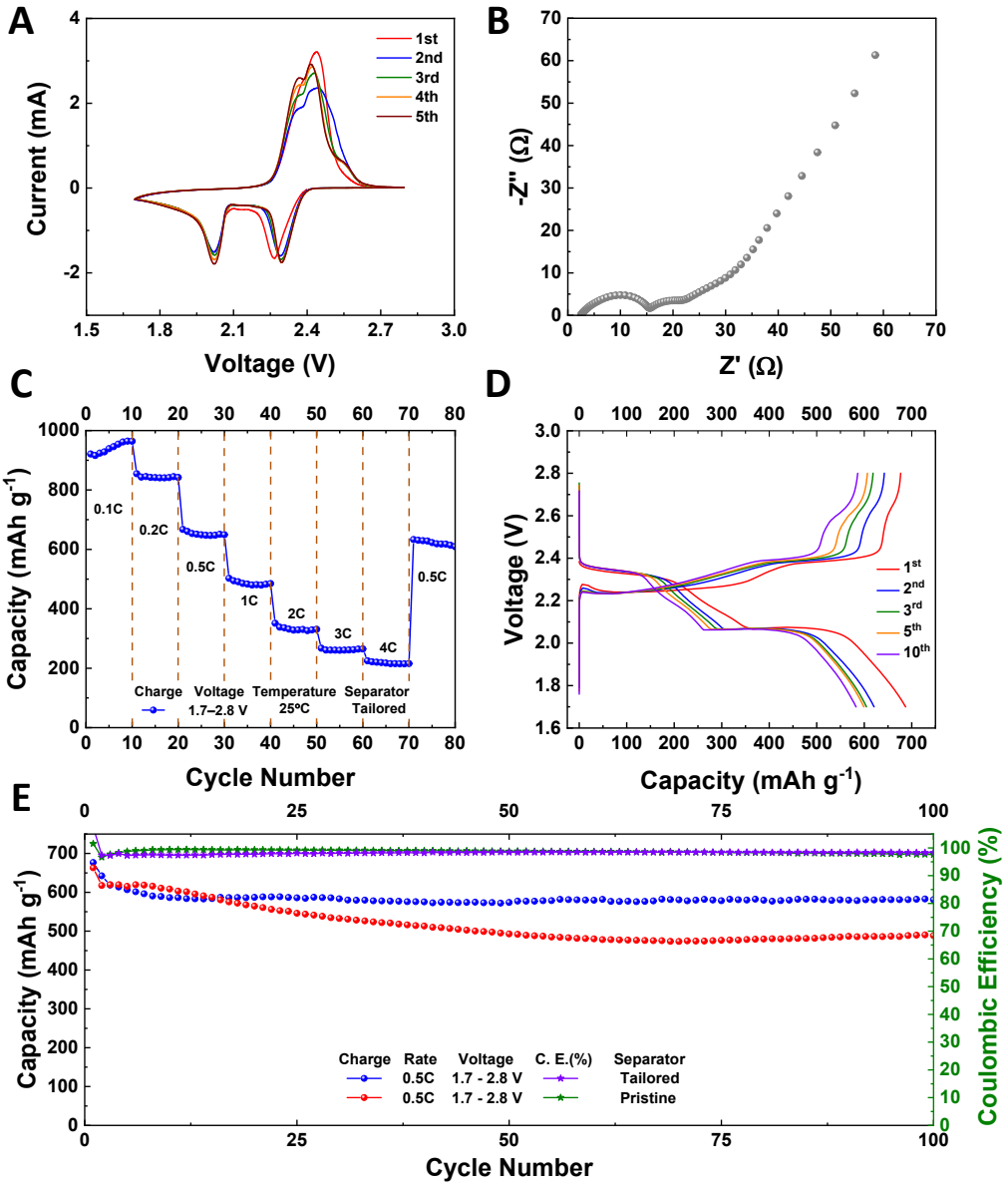

Figure 3: Electrochemical performance of Li-S cell. A: Cyclic voltammetry of Li-S cell with tailored separator at 25 ℃; B: EIS of Li-S cell with tailored separator; C: Rate studies exhibiting performance at 0.1C, 0.2C, 0.5C, 1C, 2C, 3C, and 4C at 25 ℃; D: Voltage characteristics of Li-S cells; and E: Cycling performance at 0.5C at 25 ℃.

Energy-dense batteries would be expected to play important role in performance-critical applications. Conventional LIBs present tough challenges viz., low capacity, massive overpotential, and rate capabilities at low temperatures. In such cases, Li-S batteries could play a major role as the primary reason why the batteries perform poorly at low temperatures is due to electrolyte and the co-solvents of Li-S batteries viz., DME and DOL have substantially low freezing points of –58 ℃ and –95 ℃, respectively. This allows for the conduction of lithium ions at such low temperatures. As can be seen from Fig. 2F, the conductivity of electrolyte at –25 ℃ is >5 mS cm^{-1}. A startling performance was observed for cells at 0 ℃ for the tailored separator, as shown in Fig. 4A, with the voltage characteristics resembling that of 25 ℃ performance. The two distinct discharge plateaus were observed at 2.38 V and 2.02 V. Short-chain polysulfides contribute to the majority of the capacity for Li-S system, and it can be observed that as the temperature drops down, the formation of short-chain polysulfides is suppressed resulting in lower specific capacity than 25 ℃. However, the cyclability of the tailored separator at 0.5C exhibits a stable cycling performance with an average capacity of about 392 mAh g^{-1} for 200 cycles. The performance of SC cathode at –25 ℃ was phenomenal at C/25 rate. Figure 4C demonstrates the voltage profile at –25 ℃, wherein there is drastic transformation compared to the at 25 ℃ and 0 ℃. This visible stunted suppression of the second plateau region occurs due to aggregation behavior and degree of coordination of dominant electroactive polysulfide species Li_2S_4. This behavior at –25 ℃ causes the clustering of aggregates in the electrolyte and inhibits the further conversion of the polysulfides. Another possible explanation for this behavior at low temperatures may arise from the electrostatic interaction of Li^+ cation with salt anion and polysulfides. The affinity of Li^+ towards polysulfides leads to the networking of Li^+–S_x^{-2} and thus promotes clustering. Strong coordinating lithium salts can help support Li_2S_4 conversion to Li_2S and mitigate the clustering effect.[49] Nonetheless, a specific capacity of about 170 mAh g^{-1} was obtained with >99% coulombic efficiency at –25 ℃ (shown in Fig. 4D), which is still higher than extractable from conventional LIBs. The presence of a tailored separator apart from blocking the diffusion process, reinforced in achieving a high coulombic efficiency. In general, there is huge potential in empowering the Li-S battery for critical low-temperature conditions.

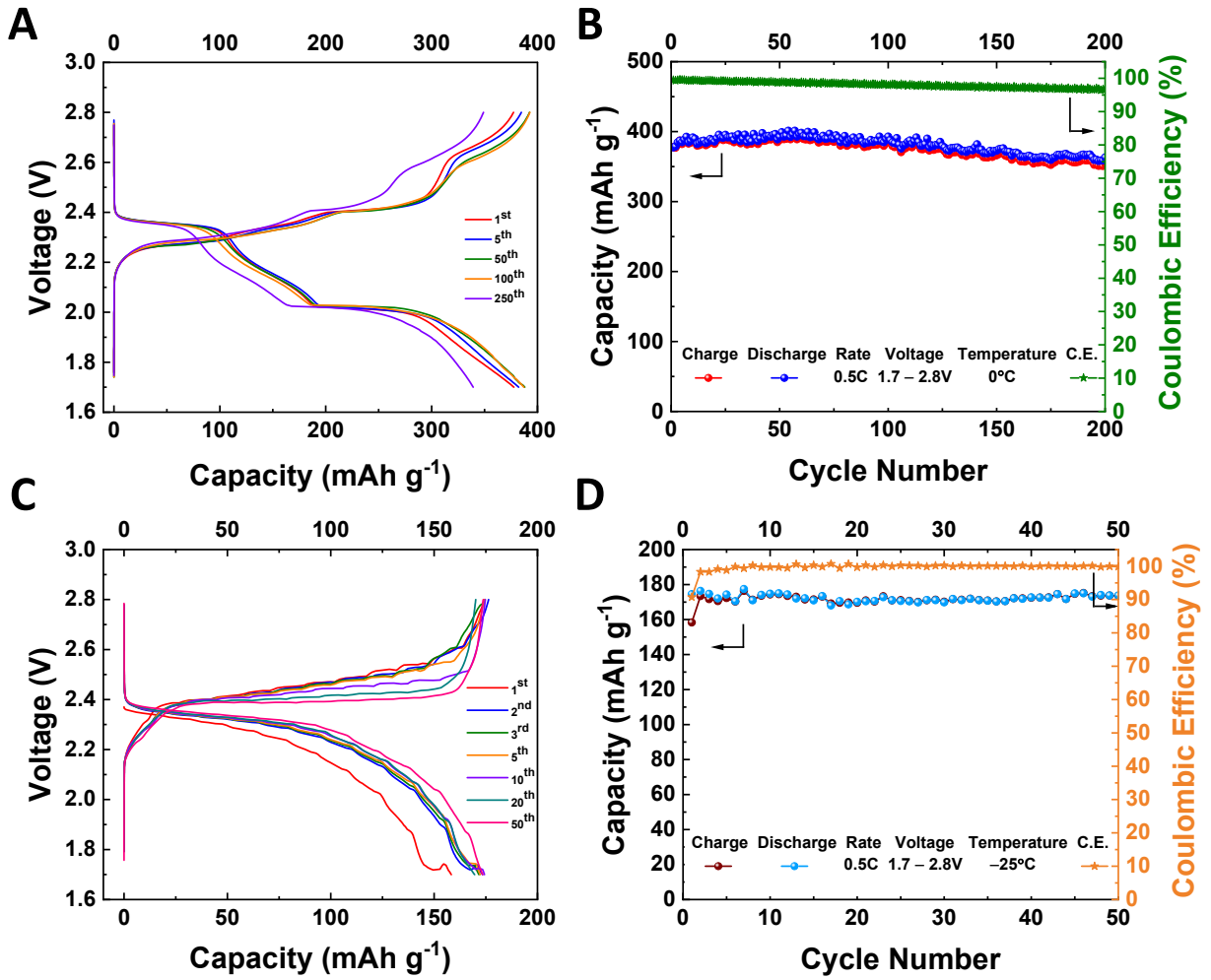

Figure 4: Electrochemical performance of Li-S cell at zero and negative temperatures. A: Voltage characteristics of Li-S cells at 0 ℃; and B: Cycling performance at 0.5C at 0 ℃; C: Voltage characteristics of Li-S cells at –25 ℃; and D: Cycling performance at 0.5C at –25 ℃

High operating temperature for Li-S batteries promotes high polysulfide shuttling due to enhanced diffusion and kinetics parameters that lead to poor life cycles. These limitations have restricted the realization of Li-S batteries for temperature-critical applications. However, the presence of the tailored separator should suppress the shuttling effect even at higher temperatures. To test the hypothesis, the cells were operated at 50 ℃ for 100 cycles, and then the temperature was reduced to 40 ℃. The electrochemical performance of the system with the tailored separator is shown in Fig. 5. At elevated temperature, charge transfer resistance decreases, which can be seen in Fig. 5A, where R_s was observed to be 5.35 Ω and R_{ct} was 4.65 Ω. After 100 cycles, at 40 ℃, R_S and R_{CT} were observed to be about 6.25 Ω and 5.99 Ω, respectively. The dual semicircle of R_{ct} may occur from PDA reducing the pore size and leading to little hindrance to ions while neighboring

graphene enhances electronic conductivity. The voltage profile of the SC cathode as seen in Fig. 5B, resembles the ones observed for 25 ℃ and 0 ℃. The two plateaus during the discharge process were seen at 2.31 V and 2.06 V. Due to the faster kinetics, there is a slight reduction in the polarization compared to 25 ℃ and 0 ℃. On subsequent cycling, the polarization reduces even further at 40 ℃. The galvanostatic cycling demonstrated stable cycling at 50 ℃ followed by 40 ℃ (Fig. 5C). At 50 ℃ the SC cathode provided the initial capacity of 604 mAh g^{-1} and 499 mAh g^{-1} after 100 cycles. The coulombic efficiency was slightly lower than 99% indicating either side reactions occurrence or a minor polysulfide shuttle effect. After 100 cycles, the capacity went to 400 mAh g^{-1} possibly due to enhanced kinetics at elevated temperature causing more polysulfide generations with ~79% capacity retention after 300 cycles. The coulombic efficiency was maintained at >98.5%

Evaluating the performance of energy material in larger configuration cells viz., pouch cell is a stepping stone towards the realization for potential applications. Pouch cells have challenges in terms of larger areal capacity, which causes severe shuttling of polysulfides, and large areal current on the Li anode that leads to dendrite growth. Both these are detrimental to the practical realization of the Li-S batteries. The presence of tailored separator aids in suppressing PS and uniformly distributing large areal current on Li anode. Figure 5D shows the performance of Li-S pouch cell, which delivered an average capacity of 541 mAh g^{-1} with coulombic efficiency >98%.

Figure 5: Electrochemical performance of Li-S cell at high temperatures of 40 ℃ and 50 ℃. A: EIS of Li-S cell with tailored separator; B: Voltage characteristics of Li-S cells at 50 ℃ and 40 ℃; C: Cycling performance at 0.5C for 100 cycles at 50 ℃ followed by 300 cycles at 40 ℃. D. Pouch cell Li/Graphene-PD-PP/CS

3. Conclusion

A tailored separator consisting of graphene–polydopamine coated on polypropylene was used to enhance the performance of Li-S batteries consisting of SC composite cathode and Li anode. The separator served multipurpose viz., blocked pathways for polysulfides shuttling with their preferential adsorption at graphene-PDA layer, enhanced electrical conductivity of SC cathode, and prevented the growth of dendrites by a uniform distribution of the areal current applied. The three critical issues of Li-S batteries were tackled using this approach. The electrochemical performance of the system was studied at –25 ℃, 0 ℃, 25 ℃, 40 ℃, and 50 ℃ and achieved stable cycling with specific capacity 170, 392, 580, 360, and 550 mAh g^{-1}, respectively. The presence of the tailored separator helped achieve stable 400 cycles at high temperatures when diffusion and kinetics are enhanced. The system had capacity retention of ~95% at 0.5C after exposure to high rates of 4C. Single-layered pouch cell delivered a capacity of 541 mAh g^{-1} at 0.5C. This strategic and promising approach will help in the advancement toward the commercialization of Li-S batteries.

4. Experimental Section

4.1 Preparation of CCS: Sulfur powder (Sigma Aldrich), carbon black (Timken Co.), PVdF HSV900 (Arkema) were taken in a ratio of 60:30:10. The sulfur powder was hand-milled with carbon black for 1 h. The mixture was then mixed with 10% w/w HSV900 binder in N-methyl pyrrolidone solvent. The slurry was mixed in Thinky planetary mixed for 40 mins at 2000 rpm. To achieve the desired loading, an appropriate wet gap was chosen, and the slurry was cast on the carbon-coated aluminum current collector. The laminate was dried in fumehood for 30 minutes and then in a vacuum oven at 50 ℃ for 3 h. The dried laminate was calendered for desired porosity of 35-40% and then punched into the electrode discs. The loading weight of the electrodes was ~3 mg cm^{-2}.

4.2 Preparation of PDA-tailored separator: The surface functionalization of the pristine separator was completed by submerging it into the dopamine solution (10×10^{-3} m), which was prepared from Tris-buffer solution (pH 8.5) and methanol, similar to previous literature.[39, 40] After 5 h, the treated separator was removed from the solution, and washed with sufficient deionized water. The tailored separator was dried in the vacuum oven at 50 °C for 20h.

4.3 Preparation of Graphene Layer Deposited PDA-Separator (PDA/ Gr-CMC Separator): As to the preparation of aqueous slurry for graphene coating, 90 mg graphene nanosheet powder (graphene-supermarket, lateral particle thickness size of ≤ 7 μm with an average flake thickness of 60 nm and specific surface area of ≤ 40 m^2/g) and 10 mg CMC binder (sigma Aldrich) were dispersed in DI water by a planetary mixer (Thinky). The prepared graphene-CMC (Gr-CMC) slurry was thinly cast onto the PDA-separator and then dried in the vacuum oven at 50 °C for 20 h. number

4.4 Preparation of single-layered pouch cells: The electrodes dimensions were 6.6 × 3.8 cm^2 with areal loading of ~2 mg cm^{-2}. The separator dimensions were 6.9 × 4.2 cm^2. The electrolyte quantity added was ~20 μL mg^{-1}. The tailored separator with graphene-PDA faced SC composite cathode. The total capacity of the single-layered pouch cell was ~20 mAh. Pouch cells were prepared in dry-room with humidity <1%, temperature ~18 ℃, and dew point temperature set at –40 ℃.

4.5 Electrochemical Characterization: After the laminate is dried, circular electrodes of 14.9 mm diameter were punched and stored under vacuum before assembling CR2032 coin cells (MTI Corporation) to study the electrochemical behavior. The cell construction was done in inert conditions inside the glovebox, which is filled with 99.998% argon having O_2 and H_2O concentration <1 ppm. Cells comprised of the SC cathode, electrolyte, Celgrad® 2500 separator, and Li anode. The electrolyte consisted of 1% w/w $LiNO_3$ in 1 M LiTFSI dissolved in 1:1 DOL/DME solution. Using Arbin cycler, galvanostatic cycling was performed within the voltage range of 1.7 – 2.8 V and the current rate of 0.1C, 0.2C, 0.5 C, 1C, 2C, and 4C. To determine the cycle stability of the SC composite, a constant current rate of 0.5C was applied. The specific capacities were determined from the active ingredient weight of the electrodes (the weight of HSV900 PVdF binder and carbon black C65 were excluded). Gamry-600 reference system was used for performing cyclic voltammetry and electrochemical impedance spectroscopy. CV was measured at a scanning rate of 0.2 mV s^{-1} from 1.7 V to 2.8 V, while EIS measurements after cell construction was recorded through 10 mV amplitude AC voltage perturbation operated over the frequency range 1 MHz – 0.01 Hz. All the potentials mentioned are versus Li^+/Li.

Acknowledgment

VP truly thanks the financial support from the Office of Naval Research (Grant # N000142112070 and Program Manager, Maria Medeiros). The authors would like to thank Dr. Anaba Anani, BrightVolt Inc. for facilitating the pouch cells construction.

References

1. J.M. Tarascon and M. Armand, *Nature* **2001**, 414(6861): p. 359-367.

2. J.B. Goodenough and K.-S. Park, *Journal of the American Chemical Society* **2013**, 135(4): p. 1167-1176.

3. A. Eftekhari and D.-W. Kim, *Journal of Materials Chemistry A* **2017**, 5(34): p. 17734-17776.

4. H. Wu and Y. Cui, *Nano Today* **2012**, 7(5): p. 414-429.

5. M. Gaberscek, M. Bele, J. Drofenik, R. Dominko, and S. Pejovnik, *Electrochemical and Solid-State Letters* **2000**, 3(4): p. 171-173.

6. M. Armand and J.M. Tarascon, *Nature* **2008**, 451(7179): p. 652-657.

7. G. Gabrielli, M. Marinaro, M. Mancini, P. Axmann, and M. Wohlfahrt-Mehrens, *Journal of Power Sources* **2017**, 351: p. 35-44.

8. M.H. Parekh, A.D. Sediako, A. Naseri, M.J. Thomson, and V.G. Pol, *Advanced Energy Materials* **2019**.

9. J. Kasnatscheew, T. Placke, B. Streipert, S. Rothermel, R. Wagner, P. Meister, I.C. Laskovic, and M. Winter, *Journal of The Electrochemical Society* **2017**, 164(12): p. A2479-A2486.

10. J.B. Goodenough and Y. Kim, *Chemistry of Materials* **2010**, 22(3): p. 587-603.

11. Q. Zhang, H. Wan, G. Liu, Z. Ding, J.P. Mwizerwa, and X. Yao, *Nano Energy* **2019**, 57: p. 771-782.

12. P.J.H. Kim, K. Kim, and V.G. Pol, *Carbon* **2018**, 131: p. 175-183.

13. P.J. Kim and V.G. Pol, *Advanced Energy Materials* **2018**, 8(36): p. 1802665.

14. W. Xue, Z. Shi, L. Suo, C. Wang, Z. Wang, H. Wang, K.P. So, A. Maurano, D. Yu, Y. Chen, L. Qie, Z. Zhu, G. Xu, J. Kong, and J. Li, *Nature Energy* **2019**, 4(5): p. 374-382.

15. A. MANTHIRAM, Y. FU, and Y.-S. SU, *Accounts of Chemical Research* **2013**, 46(5): p. 1125–1134.

16. N.H.Z.H.L.C.J.W.X.Y. Qiang Zhang, *Journal of Energy Chemistry* **2020**, 40(1): p. 151-155.

17. J. Wu, S. Liu, F. Han, X. Yao, and C. Wang, *Advanced Materials* **2021**, 33(6): p. 2000751.

18. S. Deng, X. Shi, Y. Zhao, C. Wang, J. Wu, and X. Yao, *Chemical Engineering Journal* **2022**, 433: p. 133683.

19. R. Sahore, B.D.A. Levin, M. Pan, D.A. Muller, F.J. DiSalvo, and E.P. Giannelis, *Advanced Energy Materials* **2016**, 6(14).

20. L. Borchardt, M. Oschatz, and S. Kaskel, *Chemistry* **2016**, 22(22): p. 7324-51.

21. A. Eftekhari and Z. Fan, *Materials Chemistry Frontiers* **2017**, 1(6): p. 1001-1027.

22. Y. Xia, B. Wang, X. Zhao, G. Wang, and H. Wang, *Electrochimica Acta* **2016**, 187: p. 55-64.

23. H. Wang, D. Ren, Z. Zhu, P. Saha, H. Jiang, and C. Li, *Chemical Engineering Journal* **2016**, 288: p. 179-184.

24. R.V. Bugga, S.C. Jones, J. Pasalic, C.S. Seu, J.-P. Jones, and L. Torres, *Journal of The Electrochemical Society* **2016**, 164(2): p. A265-A276.

25. B. Campbell, J. Bell, H.H. Bay, Z. Favors, R. Ionescu, C.S. Ozkan, and M. Ozkan, *Nanoscale* **2015**, 7(16): p. 7051-5.

26. Z. Gong, Q. Wu, F. Wang, X. Li, X. Fan, H. Yang, and Z. Luo, *RSC Advances* **2015**, 5(117): p. 96862-96869.

27. A. Eftekhari, L. Li, and Y. Yang, *Journal of Power Sources* **2017**, 347: p. 86-107.

28. Z.A. Ghazi, L. Zhu, H. Wang, A. Naeem, A.M. Khattak, B. Liang, N.A. Khan, Z. Wei, L. Li, and Z. Tang, *Advanced Energy Materials* **2016**, 6(24).

29. H. Park and D.J. Siegel, *Chemistry of Materials* **2017**, 29(11): p. 4932-4939.

30. D.A. Boyd, *Angew Chem Int Ed Engl* **2016**, 55(50): p. 15486-15502.

31. W.J. Chung, J.J. Griebel, E.T. Kim, H. Yoon, A.G. Simmonds, H.J. Ji, P.T. Dirlam, R.S. Glass, J.J. Wie, N.A. Nguyen, B.W. Guralnick, J. Park, A. Somogyi, P. Theato, M.E. Mackay, Y.E. Sung, K. Char, and J. Pyun, *Nat Chem* **2013**, 5(6): p. 518-24.

32. A. Eftekhari, *Sustainable Energy & Fuels* **2017**, 1(1): p. 14-29.

33. A. Abouimrane, D. Dambournet, K.W. Chapman, P.J. Chupas, W. Weng, and K. Amine, *J Am Chem Soc* **2012**, 134(10): p. 4505-8.

34. H. Wu, D. Zhuo, D. Kong, and Y. Cui, *Nat Commun* **2014**, 5: p. 5193.

35. J. He, Y. Chen, and A. Manthiram, *Energy & Environmental Science* **2018**, 11(9): p. 2560-2568.

36. B. Yu, D. Chen, Z. Wang, F. Qi, X. Zhang, X. Wang, Y. Hu, B. Wang, W. Zhang, Y. Chen, J. He, and W. He, *Chemical Engineering Journal* **2020**, 399: p. 125837.

37. W. Lin, Y. Chen, P. Li, J. He, Y. Zhao, Z. Wang, J. Liu, F. Qi, B. Zheng, J. Zhou, C. Xu, and F. Fu, *Journal of The Electrochemical Society* **2015**, 162(8): p. A1624-A1629.

38. X. Zhang, F. Ma, K. Srinivas, B. Yu, X. Chen, B. Wang, X. Wang, D. Liu, Z. Zhang, J. He, and Y. Chen, *Energy Storage Materials* **2022**, 45: p. 656-666.

39. M.H. Ryou, Y.M. Lee, J.K. Park, and J.W. Choi, *Adv Mater* **2011**, 23(27): p. 3066-70.

40. M.-H. Ryou, D.J. Lee, J.-N. Lee, Y.M. Lee, J.-K. Park, and J.W. Choi, *Advanced Energy Materials* **2012**, 2(6): p. 645-650.

41. W. Weng, V.G. Pol, and K. Amine, *Adv Mater* **2013**, 25(11): p. 1608-15.

42. A.D. Dysart, J.C. Burgos, A. Mistry, C.-F. Chen, Z. Liu, C.N. Hong, P.B. Balbuena, P.P. Mukherjee, and V.G. Pol, *Journal of The Electrochemical Society* **2016**, 163(5): p. A730-A741.

43. M.H. Parekh, B. Li, M. Palanisamy, T.E. Adams, V. Tomar, and V.G. Pol, *ACS Applied Energy Materials* **2020**.

44. Q. Zhao, X. Liu, J. Zheng, Y. Deng, A. Warren, Q. Zhang, and L. Archer, *Proc Natl Acad Sci U S A* **2020**, 117(42): p. 26053-26060.

45. C. Zhou, J. Wang, X. Zhu, K. Chen, Y. Ouyang, Y. Wu, Y.-E. Miao, and T. Liu, *Nano Research* **2021**, 14(5): p. 1541-1550.

46. M. Weiss, R. Ruess, J. Kasnatscheew, Y. Levartovsky, N.R. Levy, P. Minnmann, L. Stolz, T. Waldmann, M. Wohlfahrt-Mehrens, D. Aurbach, M. Winter, Y. Ein-Eli, and J. Janek, *Advanced Energy Materials* **2021**.

47. Z. Zhang, Z. Zhang, J. Li, and Y. Lai, *Journal of Solid State Electrochemistry* **2015**, 19(6): p. 1709-1715.

48. H. Wang, W. Zhang, J. Xu, and Z. Guo, *Advanced Functional Materials* **2018**, 28(38).

49. A. Gupta, A. Bhargav, J.P. Jones, R.V. Bugga, and A. Manthiram, *Chem Mater* **2020**, 32(5): p. 2070-2077.